Survey of the extracellular matrix architecture across the rat arterial tree

Dylan D. McCreary, MS,[a,b] Nolan F. Skirtich, BS,[a,b] Elizabeth A. Andraska, MD, MS,[a] Edith Tzeng, MD,[a,b] *and* Ryan M. McEnaney, MD,[a,b] *Pittsburgh, Pa*

ABSTRACT

Objective: To understand arterial remodeling and the pathophysiology of arterial diseases, it is necessary to understand the baseline qualities and variations in arterial structure. Arteries could differ in wall thickness, laminar structure, and laminar fenestration depending on their position within the arterial tree. We endeavored to evaluate and compare the extracellular matrix structure of different arteries throughout the arterial tree, from the aorta to the adductor muscle arteriole, with a particular focus on the internal elastic lamina (IEL).

Methods: Arterial segments were harvested from male Sprague-Dawley rats and imaged using multiple modalities. En face scans by multiphoton microscopy were used to compare native-state adventitial collagen undulation and IEL fenestration.

Results: Collagen undulation was similar across most examined arteries but straighter in the skeletal muscle arterioles ($P <$ .05). The elastic lamellae showed several differences. The IEL fenestrae were similar in average size among abdominal aorta and celiac, renal, common iliac, and common femoral arteries (range, 14-24 μm^2), with wide within-vessel variance (square of the standard deviation, 462-1904 μm^4). However, they tended to be smaller (9.08 μm^2) and less variable (square of the standard deviation, 88.3 μm^4) in the popliteal artery. Fenestrae were greater in number in the superior mesenteric artery (SMA; 6686/mm^2; $P <$ .05) and profunda femoris artery (PFA; 11,042/mm^2; $P <$ .05) compared with the other examined vessels, which ranged in surface density from 3143/mm^2 to 4362/mm^2. The SMA and PFA also showed greater total fenestration as a proportion of the IEL surface area (SMA, 15.04%; $P <$ .05; PFA, 24.11%; $P <$ .001) than the other examined arteries (range of means, 4.7%-9.4%). The arteriolar IEL was structurally distinct, comparable to a low-density wireframe. Other structural differences were also noted, including differences in the number of medial lamellae along the arterial tree.

Conclusions: We found that vessels at different locations along the arterial tree differ in structure. The SMA, PFA, and intramuscular arterioles have fundamental differences in the extracellular matrix structure compared with other arteries. Location-specific features such as the medial lamellae number and elastic laminar structure might have relevance to physiology and confer vulnerabilities to the development of pathology. (JVS—Vascular Science 2022;3:1-14.)

Clinical Relevance: Arterial pathologies affect and depend on elastic fibers and collagen. Medial arterial calcification involves mineral deposition onto elastic fibers and smooth muscle cell osteogenesis, which can be induced by elastin degradation. Degradation or remodeling of the extracellular matrix can be a critical component of atherosclerosis and hypertension. Pathologies can also be site-specific. Aneurysms are most common in the abdominal aorta (Ao), followed by the popliteal artery, which shows age-related changes to wall properties comparable to those in central elastic arteries. Visceral artery aneurysms, however, are rare. Location differences in arterial extracellular matrix structure could inform site-specific differences in arterial pathology.

Keywords: Arteries; Arterioles; Elastic tissue; Extracellular matrix; Fibrillar collagens

The extracellular matrix (ECM) accounts for the structural stability and static mechanical properties of arteries. Two of the most abundant components of the vascular ECM are elastic and collagen fibers. The elastic fibers provide resilience and energy distribution and storage under normal physiologic parameters and the collagen fibers

From the Department of Surgery, University of Pittsburgh School of Medicine[a]; and the Department of Surgical Service, Veterans Affairs Pittsburgh Healthcare System.[b]

The present project was funded in part by Vascular Cures (to R.M.M.), the U.S. Department of Veterans Affairs (grant IK2BX003509 to R.M.M.), the National Heart, Lung, and Blood Institute (grant 5T32HL0098036 to E.A.A.), and a Physician-Scientist Institutional Award from the Burroughs Wellcome Fund held by the University of Pittsburgh (to E.A.A.).

Author conflict of interest: none.

Presented as an early version at a QuickShot Session at the 15th Annual Academic Surgical Congress, Orlando, Fla, February 4-6, 2020.

Correspondence: Ryan M. McEnaney, MD, Department of Surgery, University of Pittsburgh Medical Center, UPMC Presbyterian South Tower, 3rd Floor, Rm E351.5, 200 Lothrop St, Pittsburgh, PA 15213 (e-mail: mcenaneyrm@upmc.edu).

The editors and reviewers of this article have no relevant financial relationships to disclose per the JVS-Vascular Science policy that requires reviewers to decline review of any manuscript for which they may have a conflict of interest.

2666-3503

https://doi.org/10.1016/j.jvssci.2021.08.001

provide rigid structural support.[1] When increasing wall strain is applied, the adventitia, which is largely composed of type I collagen, prevents overdistension and damage to the arterial wall.[1] Combined, elastic and collagen fibers represent ~50% of the dry weight of arteries and confer the characteristic "nonlinear elasticity" that is vital to the function of a closed circulatory system.[2,3]

Elastic fibers are composite materials that consist of peripherally oriented fibrillar proteins and proteoglycans surrounding a dense, heavily crosslinked core of elastin protein. Elastic fibers are incredibly durable, with an estimated half-life approaching the human lifespan.[4] These fibers appear to be created predominantly in development, with very little new elastin synthesis in adult tissues.[5] Elastic fibers are present throughout the arterial wall but consolidate to form dense, sheet-like lamellae in the tunica media and internal elastic lamina (IEL), which borders the tunica intima. In large elastic arteries, the IEL is a thick sheet of densely packed elastic fibers oriented parallel to the axis of flow, poised best to support longitudinal stresses.[6] Elastic lamellae such as the IEL are frequently interrupted by fenestrations, which serve as windows for small molecule transport and cell—cell communication.[7-10] Collagen fibers have a short half-life compared with that of elastic fibers, especially under strain, such as occurs in hypertension, and require continual synthesis for replacement.[11] Adventitial collagen fibers are oriented in a double helical pattern around the axis of the vessel, with the waviness dependent on the applied tension.[12,13] The mechanical properties, durability, and distribution of elastic and collagen fibers are important to the function of arteries and have roles in pathologies such as aneurysmal disease, atherosclerosis, and medial calcification and in physiologic arterial wall remodeling.

Collagen and elastin structures can be differentiated within vascular tissues using multiphoton microscopy (MPM).[14-17] The method relies on the optical properties of the fibrillar proteins and does not require tissue staining or fixation, making it ideal for evaluation of native structural morphology.[18] In the present study, we examined the collagen and elastic fiber morphology among healthy rat arteries isolated throughout the arterial tree. We used MPM to create high-resolution image volumes of arterial ECM to compare the baseline collagen and elastic fiber architecture from arteries that exist in different locations along the arterial tree. We have included a discussion of the implications of the morphologic distinctions.

ARTICLE HIGHLIGHTS

- **Type of Research:** Basic science
- **Key Findings:** Superior mesenteric and profunda femoris arteries have more internal elastic lamina fenestrae on average than other arterial locations. Popliteal arteries have smaller fenestrations with less size variability. Arterioles demonstrated a low-density wireframe for elastic structure and straighter adventitial collagen fibers compared with other arteries.
- **Take Home Message:** Vessels at different locations along the arterial tree differ in their baseline structure. Features such as medial lamellae quantity and internal elastic laminar architecture might have physiologic relevance and confer vulnerabilities to the development of pathology.

METHODS

Animal husbandry. All animal procedures were performed in accordance with the institutional animal care and use committee of the University of Pittsburgh (protocol no. 19095696). Forty 340- to 400-g male Sprague-Dawley rats (Envigo, Indianapolis, Ind), aged 20 to 28 weeks, were housed under pathogen-free conditions. Male rats were chosen to reduce the complications in husbandry. Rats were used instead of mice given the larger size, which generally allowed for more reliable sampling of the smaller derivative arterial branches for microscopy.

Tissue harvest. The rats were anesthetized with a mixture of 90 mg/kg of ketamine and 5 mg/kg of xylazine (Covetrus, Dublin, Ohio) and then perfused via an aortic catheter with phosphate-buffered saline (PBS; pH = 7.2) containing 200 μM adenosine, 500 μM sodium nitroprusside, and 500 μM verapamil (Sigma-Aldrich, St Louis, Mo) to induce maximal arterial vasodilation. The rats were then perfusion-fixed through the same catheter by infusing 2% paraformaldehyde in PBS (Santa Cruz Biotechnology, Santa Cruz, Calif). To visualize the hindlimb microvasculature, some of the animals were subsequently perfused with a colored silicone casting agent (MICROFIL MV120; Flow Tech Inc, Carver, Mass) prepared according to the manufacturer's specifications and allowed to cure. Arterial segments 4- to 10-mm long were carefully extracted for imaging. The extracted arteries included the abdominal aorta (Ao) and common iliac (CIA), common femoral (CFA), popliteal, renal, superior mesenteric (SMA), celiac, and profunda femoris (PFA) arteries. In addition, several second and third-order intramuscular arterioles (MscAs), which branched from the PFA or saphenous artery and are found within the substance of the adductor muscle, were extracted (Fig 1).

Human arterial specimens were isolated from discarded lower extremity surgical amputations performed for clinically advanced ischemic disease. The patients provided written informed consent to the clinical physician team for retention and analysis of the de-identified

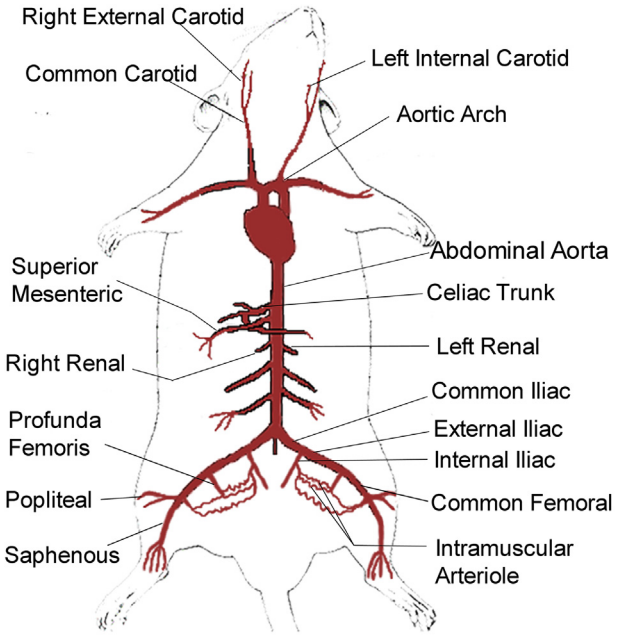

Fig 1. Diagram of the rat arterial tree. Most major arteries are labeled, in addition to those examined for our report. The examined arteries included the aorta, superior mesenteric, celiac, renal, common iliac, common femoral, profunda femoris, and popliteal arteries and intramuscular arterioles, which branched from the profunda femoris. Adapted from BiologyCorner.com[19] under a Creative Commons Attribution-NonCommercial-ShareAlike 4.0 International License.

discarded clinical specimens. The arterial tissues were harvested in accordance with the University of Pittsburgh institutional guidelines (institutional review board protocol no. PRO11070041). The arterial specimens were collected from both transtibial and transfemoral amputations and represented muscular arterioles or perineural feeding vessels. These vessels were fixed in 2% paraformaldehyde for microscopy.

Tissue processing. For en face and whole vessel imaging, the arterial segments were stored at 4°C in 0.5% paraformaldehyde after fixation. In preparation for MPM, loose connective tissue and extraneous skeletal muscle were carefully removed. For en face imaging, 1- to 2-mm-long segments were cut from the excised vessels and cut open lengthwise. The opened segments were splayed flat onto a glass slide and cover slipped with PBS as the mounting media. The edges of the slides were sealed with a light brushing of Permount (Fisher Scientific, Waltham, Mass). The slides were stored at 4°C before imaging. The small diameter and delicate structure of the MscAs prevented us from splaying them open to image en face; thus, all MscA images were obtained with a whole-vessel preparation. For the whole-vessel images, the vessel segments were placed in drop slides with 1- to 4-mm depressions, submerged in PBS, and transiently cover slipped.

For cross-sectional imaging, the arterial samples were first cryoprotected by submerging in 30% sucrose for ≥24 hours and then frozen by submersion in liquid nitrogen-cooled 2-methylbutane and stored at −80°C. The frozen samples were embedded in OCT compound (Fisher Scientific), and 6- to 9-μm-thick cross sections were cut using a cryostat at −30° to −25°C and mounted onto charged microscope slides (Fisher Scientific). The slides were stored at −80°C before staining and imaging. The cross sections to be imaged via MPM or confocal microscopy were mounted on slides using gelvatol.

Histologic examination. As an additional method of examining the collagen and elastic fiber architecture, a subset of cross sections was processed with a modification of the Verhoeff-van Gieson staining protocol (HT25A; Sigma-Aldrich). The Verhoeff-van Gieson–stained sections were imaged under bright field transillumination using RGB (red, green, blue primary colors of light) color with an Olympus AX70 (Provis) microscope (Olympus Corp, Tokyo, Japan).

A subset of cross sections was stained with DAPI (4′,6-diamidino-2-phenylindole) for 20 to 30 seconds, cover slipped using gelvatol as the mounting media, and allowed to dry at 4°C. Confocal fluorescence micrographs (1024 × 1024 pixels) of DAPI (excitation, 405 nm; emission, 461 nm) and elastic fiber (excitation, 473 nm; emission, 520 nm) autofluorescence were obtained at 20× magnification using an Fluoview FV1000 confocal microscope (Olympus, Tokyo, Japan; purchased with grant 1S10OD019973-01 awarded to Dr Simon C. Watkins) with a 0.85 NA (numeric aperture) oil immersion objective.

Multiphoton microscopy. MPM was performed using an FV1000 MPE microscope (Olympus; purchased with grant 1S10RR025676-01 awarded to Dr Simon C. Watkins) with a Chameleon ultra-mode-locked titanium/sapphire laser (Coherent, Palo Alto, Calif) set to 830 nm, through a 1.05 NA 25× water-immersion objective. The RXD1 channel (350- to 450-nm emission filter) allowed for visualization of the fibrillar collagen via second harmonic generation, and the RXD2 channel (500- to 550-nm emission filter) was used to image the elastic fiber autofluorescence via two-photon excitation. Image stacks were acquired at 1024 × 1024 pixels (508.4 × 508.4 μm) per frame with a 1-μm step-size at 8 to 10 μs/pixel exposure time. For whole vessels, a 3× line Kalman filter was applied, which uses a recursive algorithm to integrate multiple sweeps of the laser and reduce stochastic noise. For the en face images and cross sections, a 4× line Kalman integration filter was applied.

Image analysis of collagen undulation. Analysis of collagen fiber undulation was performed using ImageJ (National Institutes of Health, Bethesda, Md; Fig 2, *A*). Maximum intensity projections of image stacks of the

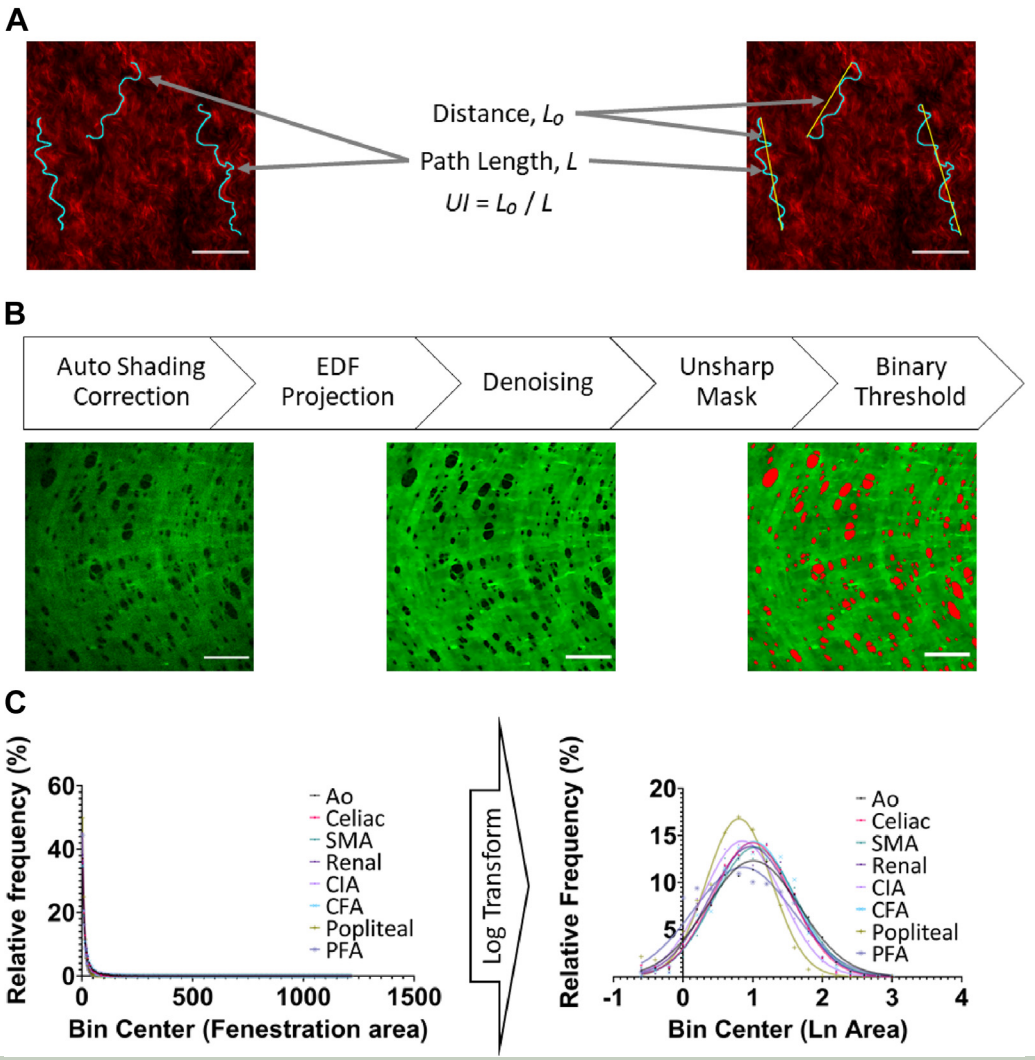

Fig 2. Image data processing. **A,** Collagen undulation. Contiguous collagen fibers were traced on maximum intensity projection of adventitial collagen (*red*). A ratio of the end-to-end distance, L_O (*yellow*) to the fiber path length, *L* (*blue*) was used to obtain the undulation index, *U*. **B,** Internal elastic lamina (IEL) fenestration analysis. Using an automated workflow, a sample image stack of the elastin underwent shading correction and then was collapsed into an extended depth of focus (*EDF*) projection, de-noised, and sharpened, before the dark spaces were selected by threshold and manual tracing, as indicated. Scale bars = 50 μm. **A,B,** Images obtained at 25× magnification. **C, Left,** Relative frequency distributions of vessel-pooled fenestrations revealing a right-skewed distribution. **C, Right,** Log transformation results in Gaussian distributions, appropriate for one-way analysis of variance. *Ao,* Abdominal aorta; *Celiac,* celiac artery; *CFA,* common femoral artery; *CIA,* common iliac artery; *PFA,* profunda femoris artery; *Popliteal,* popliteal artery; *Renal,* renal artery; *SMA,* superior mesenteric artery.

adventitial collagen were produced, and several fibers were traced freehand (path length [L]). Straight lines from end to end of the tracing were drawn to give the point-to-point distance (L_O). Finally, a ratio was computed of the distance to the path length to give an undulation index, UI (UI = L_O/L), as reported previously.[12] The UI has a maximum value of 1.0, indicating a straightened fiber. Twelve to fifteen fibers were used to compute the average UI from each image, and five to seven rats at one to two images (258,501 μm^2 frame area) per rat were used to determine the average undulation value for a given vessel type. The collagen fibers were traced from the en face images, if possible, but were obtained from whole-vessel preparations of the MscAs.

Image analysis of IEL fenestrae. Analysis of IEL fenestrae was performed using Nikon NIS Elements, version 5.21.01 (Nikon, Tokyo, Japan; Fig 2, *B*). Analysis was performed on one to two image stacks per vessel segment. Image stacks were cropped in *z* to the 6 to 12 frames depicting the IEL and then in *xy* to exclude the darker image periphery, leaving the central 150,000 to 200,000 μm^2 space. The shading of the stack was then corrected to accommodate for brightness variability.

Extended-depth-of-focus projections were made from the corrected frames, and the resulting projections were de-noised and sharpened via unsharp masking. The processing was partially automated using the general analysis 3 feature. A binary threshold was defined to select the dark spots in the image (Fig 2, *B*). Objects were manually redrawn, as necessary. One or more regions of interest (ROIs) were then drawn to select most of the image area, excluding the low-contrast spaces, visible wrinkles, and other imaging artifacts. Automated measurements of the object surface area and count, binary area, ROI area, and binary fraction were performed. The binary area refers to the total surface area of the selected objects (fenestrations). The binary fraction indicates the total fenestrated space as a proportion of the ROI space. The number of objects was divided by the ROI size to determine the fenestration density (number of objects/mm^2). Finally, the variance (square of the standard deviation [SD^2]) of object surface area for a given image was used as a measure of fenestration size variability.

Statistical analysis. Five to seven rats were analyzed for each vessel classification. The collagen tissue UIs were analyzed via one-way analysis of variance (ANOVA), with individual comparisons via Tukey's honestly significant difference (HSD) with *P* value correction for multiple comparisons. The distribution of fenestration sizes (object area) for an artery was consistently right-skewed, with most fenestrations being small. The first-run statistical analyses further indicated that the data did not fit a Gaussian model. Therefore, the raw fenestration areas, total fenestration, and density were log-transformed [Y* = Ln (Y)]. The resulting distributions fit a Gaussian model and could thus be analyzed using one-way ANOVA (Fig 2, *C*). The transformed IEL fenestration area, density, total fenestrated space, and variance of the transformed fenestration area were each analyzed using one-way ANOVA, with individual comparisons via Tukey's HSD, with *P* value correction for multiple comparisons. The fenestration data are presented untransformed, and the statistically significant differences are reported exclusively from the transformed data. All graphs and stated values are presented as the mean ± standard error of the mean. Statistical analyses were performed using GraphPad Prism 8 (GraphPad, San Diego, Calif).

RESULTS

Structural observations. The most prominent elastic structure in all arteries observed was the IEL (Fig 3, *A-C*). The medial elastic fibers intermittently coalesced into incomplete fenestrated elastic lamellae, which varied in number depending on arterial location. Circumferential cross sections of the Ao showed seven to eight dense lamellae (n = 4 rats) at our sampling region between the celiac and renal arteries, including the IEL and external elastic lamina. In contrast, the CFA had four to five layers (n = 4 rats). The thoracic aorta is known to decrease in medial lamellae as it descends, because the medial lamellae contribute to the formation of the intercostal branches, although the abdominal aorta does not decrease in lamellae.[20,21] Muscular arterial branches such as the PFA (cross sections from five rats) have less defined medial elastic lamellae, and smaller branch vessels appear to lack a defined external elastic lamina. Instead, the medial elastic fibers exist in a more filamentous form compared with the dense sheets of the aorta. We observed that the IEL wrinkles and elastic fibers orient parallel to the direction of flow. In contrast, the elastic fibers in the media are oriented perpendicular to the direction of flow (Figs 3, *D*, and 4) for all vessels. Similar findings have been previously reported from electron microscopic analysis of aorta specimens.[6]

Adventitial collagen. Although fibrillar collagen is present throughout the arterial wall, it is concentrated in the adventitia. Adventitial collagen was morphologically similar as wavy fiber bundles in all arteries examined (Fig 5, *A*). The mean UI of adventitial collagen was 0.6423 ± 0.002 and ranged from 0.516 to 0.868 for the individual vessels. The UIs were as follows (mean ± standard error of the mean): aorta (n = 5), 0.597 ± 0.017; celiac trunk (n = 5), 0.574 ± 0.023; SMA (n = 5), 0.569 ± 0.015, renal artery (n = 6), 0.671 ± 0.005; CIA (n = 5), 0.613 ± 0.028; CFA (n = 5), 0.682 ± 0.017; popliteal artery (n = 6), 0.640 ± 0.033; PFA (n = 7), 0.672 ± 0.014; and MscA (n = 5), 0.752 ± 0.043. The UI was similar for most of the vessels examined, except for the MscAs [one-way ANOVA, $F(8,24) = 2.74$; $P < .0001$], which had a slightly greater mean UI than did the Ao ($P = .002$), celiac trunk ($P = .0002$), SMA ($P = .0002$), CIA ($P = .007$), and popliteal artery ($P = .041$; Fig 5).

Internal elastic lamina. The architecture of the IEL was largely consistent across the arterial tree with some exceptions. The IEL of the Ao (n = 5), celiac artery (n = 5), SMA (n = 5), renal artery (n = 5), CIA (n = 6), CFA (n = 5), and popliteal artery (n = 5) appeared as dense, fenestrated sheets. These sheets generally featured a wrinkled or folded topology. The IEL of the PFA (n = 6) and muscular branches (n = 5 rats) was more filamentous and web-like, with a greater degree of branching from the aortic "main line" and a smaller size correlating with a more perforated and web-like appearance (Fig 6, *A*). The IEL fenestration characteristics of the various arterial segments are shown in Fig 6, *B* to *E*. On average, the arterial IEL surface area showed 10.19% ± 1.12% total fenestration. Most of the examined arteries had a total fenestration of 5% to 10% of the IEL surface area (Fig 6, *B*).

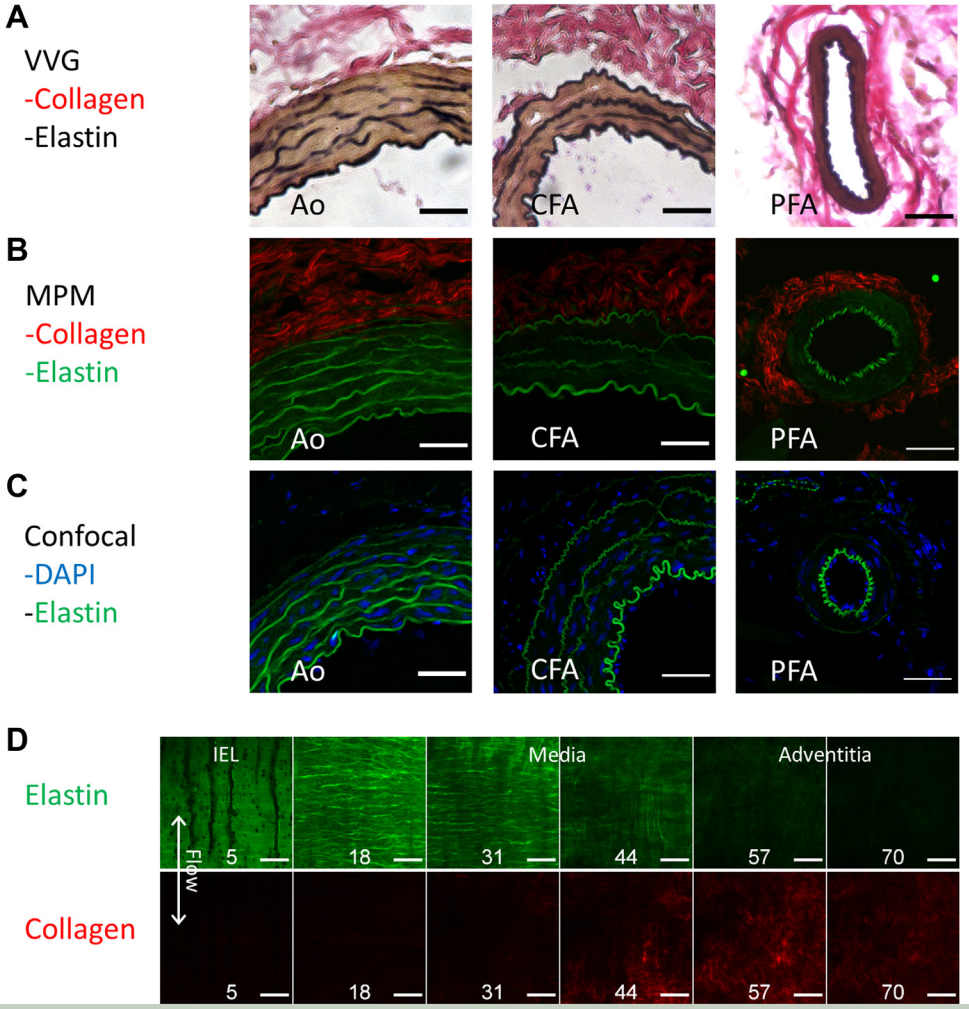

Fig 3. Laminar organization of arterial extracellular matrix (ECM). **A,** Verhoeff-van Gieson (*VVG*) staining of the abdominal aorta (Ao), common femoral artery (CFA), and profunda femoris artery (PFA). Elastic fibers were stained *black*, collagen fibers were stained *red*, and other tissue components were stained *yellow*. **B,** Maximum intensity projections of cross-sections of the Ao, CFA, and PFA obtained through multiphoton microscopy (MPM). The collagen was false-colored *red*; and the elastic fibers, *green*. **C,** Cross sections of the same types of artery using confocal microscopy stained with DAPI (4′,6-diamidino-2-phenylindole; *blue*) and showing the elastic fiber autofluorescence (*green*). **D,** Montage of an image stack of the celiac trunk viewed en face. Numbers indicate depth from the lumen (μm). Note the inverse distribution of elastic fibers (**Top**, *green*) and collagen (**Bottom**, *red*) across the layers. *Arrow* indicates the flow direction and longitudinal orientation of the artery. **A** and **C,** Images obtained at 20× magnification. **B** and **C,** Images obtained at 25× magnification. Scale bars = 50 μm.

The PFA and SMA, however, had greater fenestration than the norm [one-way ANOVA of Ln-transformed, $F(7,34) = 16.78$; $P < .0001$]. The total fenestration of the PFA (24.11% ± 3.67%) was significantly greater than that of every other artery, except for that of the SMA (Tukey's HSD, Ao, 9.43% ± 1.77%; $P = .0005$; for all others, $P < .0001$). The SMA (15.04% ± 1.40%) demonstrated significantly greater total fenestration than did the celiac artery (6.89% ± 0.547%; $P = .0098$), renal artery (6.84% ± 0.821%; $P = .007$), CIA (4.70% ± 0.780%; $P < .0001$), CFA (7.49% ± 0.789%; $P = .026$), and popliteal artery (5.65% ± 0.674%; $P = .0005$) but was not significantly different from that of the aorta (9.44% ± 1.77%) or PFA. We also found a small, but statistically significant, difference in the total fenestration of the Ao compared with the CIA ($P = .014$).

The differences in total fenestration resulted predominately from the greater surface densities of the fenestrations (Fig 6, *C*). The PFA had 11,042 ± 1104 fenestrations/mm^2, and the SMA had 6686 ± 796.5/mm^2 compared with a group average of 5476 ± 439.8 fenestrations/mm^2 [one-way ANOVA of Ln-transformed, $F(7,34) = 15.70$; $P < .0001$]. The PFA had significantly more fenestrations relative to the IEL

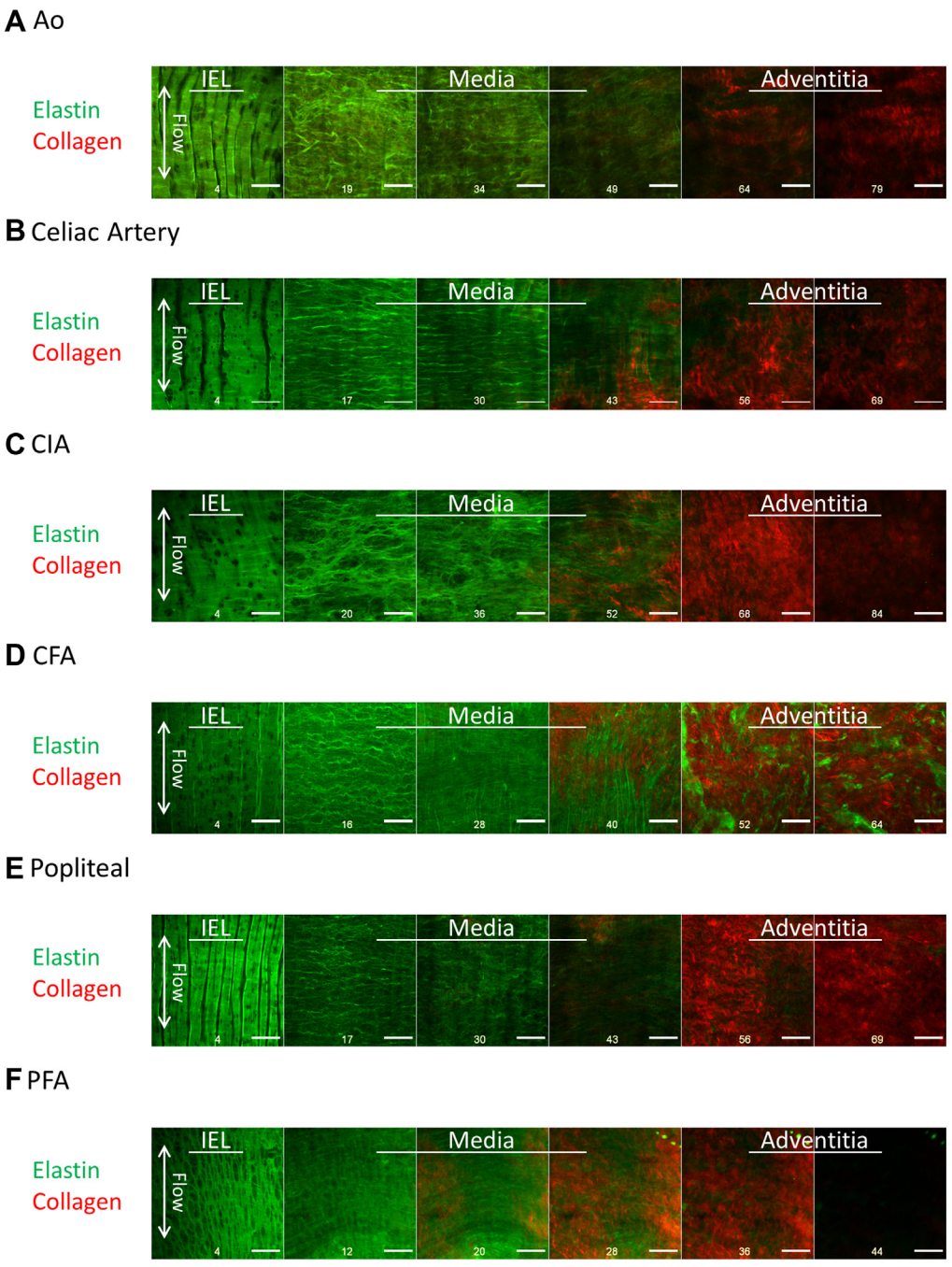

Fig 4. Variability in arterial laminar architecture. Montages of multiphoton image stacks of several example arteries viewed en face, as labeled. Numbers at the bottom indicate the depth in the radial direction from the lumen in microns. Note the clear visibility of external elastic lamina (EEL) at 40 μm depth in the common femoral artery (CFA), and the profunda femoris artery (PFA) lacks an EEL entirely. The PFA also has a thinner arterial wall. The slice intervals varied between vessels. All images were obtained at 25× magnification. Scale bars = 50 μm. *Ao,* Abdominal aorta; *CIA,* common iliac artery; *Popliteal,* popliteal artery.

surface area compared with all other examined arteries (PFA vs SMA, $P = .03$; PFA vs popliteal artery, 6325 ± 595.6/mm^2; $P = .015$; PFA vs all others, $P < .0001$). The fenestration density of the SMA was significantly greater than that of celiac artery (3907 ± 279.6/mm^2; $P = .039$), CIA (3143 ± 221.8/mm^2; $P = .0005$), and CFA (3945 ± 228.6/mm^2; $P = .049$). The popliteal artery fenestration density was also significantly greater than that of the CIA ($P = .001$). However, neither the popliteal artery nor SMA was significantly different from the renal artery (4016 ± 308.2/mm^2) or Ao (4362 ± 864/mm^2).

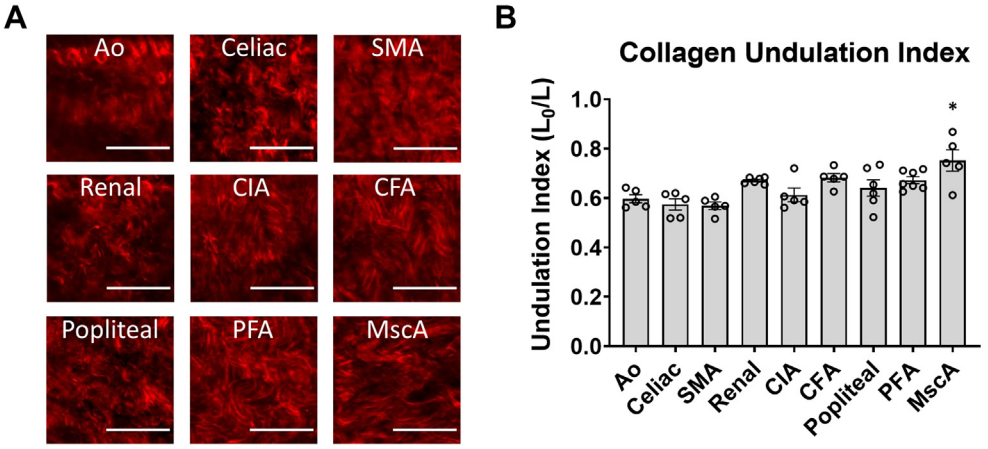

Fig 5. Undulation indexes (UIs) of adventitial collagen were similar across most of the arterial tree. **A,** Sample maximum intensity projections (*MIPs*) of the adventitial collagen of several rat arteries. Images were obtained at 25× magnification. Scale bars = 50 μm. **B,** Graph of the collagen UIs showing a small, but significantly, greater UI for intramuscular arterioles (MscAs) compared with the abdominal aorta (Ao), common iliac artery (CIA; $P < .01$), celiac artery, superior mesenteric artery (SMA; $P < .001$), and popliteal artery ($P < .05$) but no significant differences in the UI between other arteries. *Open circles* represent individual rats. One-way analysis of variance plus Tukey's honestly significant difference (HSD; *$P < .05$).

The average fenestration size was 18.45 ± 1.08 μm^2 across all arteries. The popliteal artery demonstrated somewhat smaller fenestrations (9.086 ± 0.940 μm^2, Fig 6, *D*) than the others, which were significantly smaller than those of the SMA [23.15 ± 2.06 μm^2; one-way ANOVA of Ln-transformed, $F(7,34) = 2.66$; $P = .026$; Tukey's HSD, $P = .027$]. The mean fenestration area for the other arteries were as follows: Ao, 24.49 ± 5.35 μm^2, celiac artery, 17.65 ± 0.627 μm^2; renal artery, 17.58 ± 2.95 μm^2; CIA, 14.72 ± 2.08 μm^2; CFA, 18.82 ± 0.929 μm^2; and PFA, 21.72 ± 2.56 μm^2. Within a given artery, the variance (SD^2) in fenestration size was, on average, 866.27 ± 155.88 μm^4 (relating to an average single-image standard deviation of 26.02 ± 2.12 μm^2), indicating a high degree of within-vessel variability (Fig 6, *E*). The popliteal artery showed lower variance (within vessel SD^2, 88.32 ± 16.57 μm^4), which was significantly different from that of the PFA (SD^2, 1613 ± 483 μm^4; $P = .025$). The other variances were as follows: Ao, 1904 ± 984 μm^4; celiac artery, 534 ± 47.2 μm^4; SMA, 1134 ± 178 μm^4; renal artery, 553 ± 201 μm^4; CIA, 462 ± 160 μm^4, CFA, 645 ± 194 μm^4. The other arteries were not significantly different from each other in fenestration characteristics.

Arterioles. The IEL of the smaller second and third-order MscAs could not be analyzed using the method as used for the other vessels. Most skeletal muscle arterioles (n = 18 arteriolar segments from six rats) showed an IEL similar to that of the medium-size veins, with a sparse web of elastic fibers accounting for the structure (Fig 7). The web-like structure could not be interpreted as a fenestrated sheet. The relative elastic fiber content appeared to decrease with increasing branching orders. These structures and the IEL organization bear resemblance to the small nutrient vessels removed from human lower limb specimens (Supplementary Fig).

DISCUSSION

We found arterial adventitial collagen to be structurally similar across most of the examined arteries but ~10% straighter in the MscAs, implying a greater applied tension in these vessels. The IEL structure, however, showed location-specific differences in fenestration characteristics. The SMA and PFA demonstrated greater fenestration and a larger density of fenestrae, and popliteal artery showed marginally smaller fenestrae and less fenestration variability. The IEL of the MscAs was architecturally distinct from the fenestrated sheets of the larger arteries. Although vascular smooth muscle cells (VSMCs) are prominent in the arterial wall, their elimination does not significantly change the mechanical properties of large arteries, suggesting a greater dependence on ECM components.[22] Although elastic laminae were initially thought to be continuous, amorphous sheets separated by collagen fibers and smooth muscle cells,[23] they were later found to possess a microfibrillar structure.[24,25] The adventitia is composed largely of type I collagen bundles produced by resident myofibroblasts. The wavy, ribbon-like configuration is prevalent in a relaxed state but straightens when increased wall tension is applied or when load-bearing elastic fibers are disrupted, such as in aneurysmal disease.[12,13,26]

IEL fenestrae have been shown to be plastic and to undergo significant remodeling during development and in response to fluid shear-stress conditions.[27,28] Also, variability in the IEL architecture is known between the different arteries located within the mature arterial tree. Kirby et al[10] showed a significant difference in the total

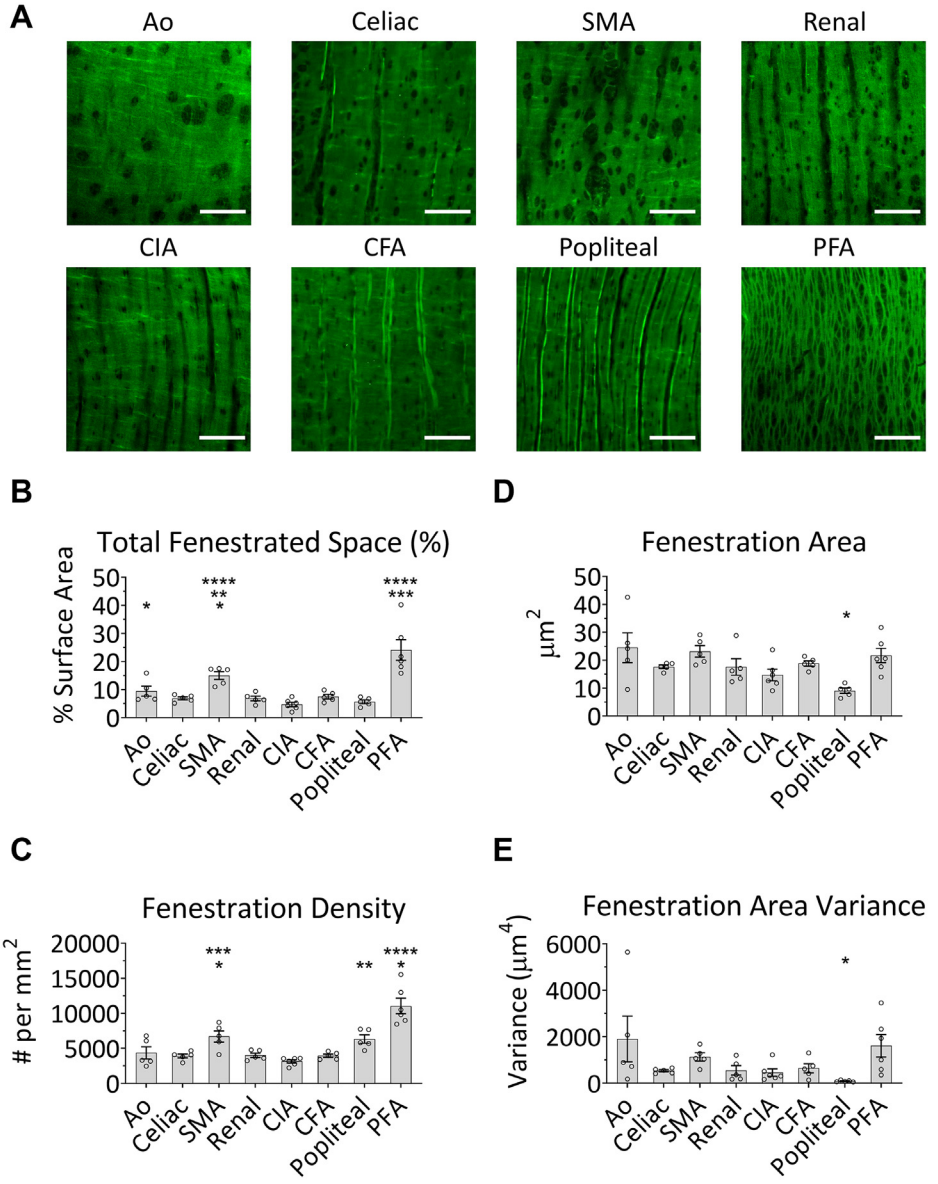

Fig 6. Analysis of internal elastic lamina (IEL) fenestrae. **A,** Sample maximum intensity projections of the internal elastic lamina (IEL) of several rat arteries viewed en face. Images were obtained at 25× magnification. Scale bars = 50 μm. **B-E,** Graphs of fenestration characteristics between arteries. The displayed data are untransformed, and *open circles* represent individual rats. Data were log-transformed and then analyzed using one-way analysis of variance (ANOVA) with Tukey's honestly significant difference (HSD) post hoc test and *P* value correction. Significant differences were as follows. *B*, The aorta had greater total fenestration than the common iliac artery (CIA; $P < .05$). The profunda femoris artery (PFA) showed greater total fenestration than all other examined arteries except for the superior mesenteric artery (SMA; abdominal aorta [Ao], $P < .001$; all others, $P < .0001$). The SMA showed greater total fenestration than all vessels, except for the Ao and PFA (vs celiac and renal arteries, $P < .01$; common femoral artery [CFA], $P < .05$; popliteal artery, $P < .001$; CIA, $P < .0001$). **C,** The PFA showed greater fenestration density than the other vessels (SMA and popliteal artery, $P < .05$; all others, $P < .0001$); the density of the SMA was significantly greater than that for the celiac artery and CFA ($P < .05$) and CIA ($P < .001$). The popliteal artery showed significant differences from the CIA ($P = .001$). **D,** The popliteal artery had significantly smaller fenestrations than did the SMA ($P < .05$). **E,** The popliteal artery demonstrated lower variability in fenestration size, which was significantly different from that of the PFA ($P < .05$). *$P < .05$, **$P < .01$, ***$P < .001$, and ****$P < .0001$.

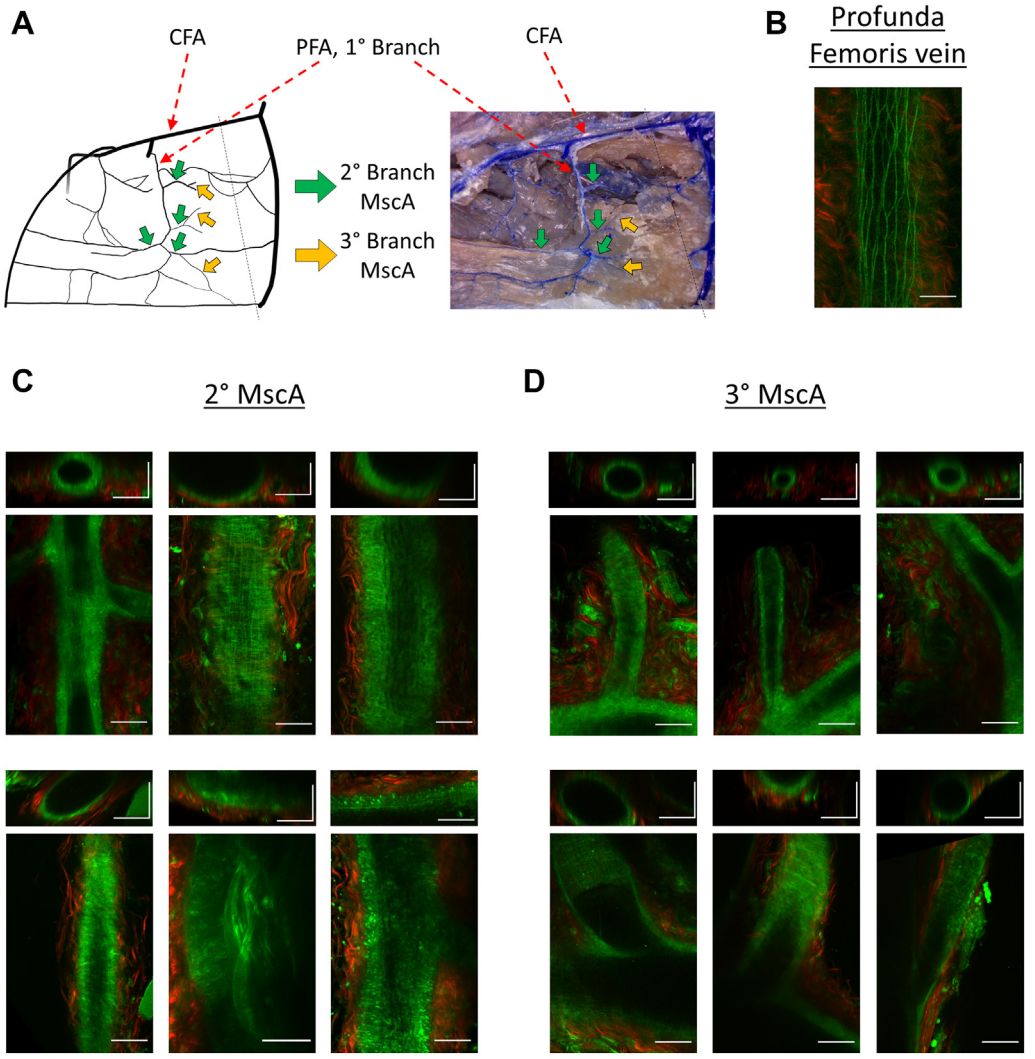

Fig 7. Skeletal muscle arteriolar internal elastic lamina (IEL) is sparse and variable. **A,** A diagram and microfil cast of rat groin arterial system. The common femoral artery (CFA) and profunda femoris artery (PFA) are indicated. The degree of branching was defined relative to the CFA. The PFA is the first-order (1°) branch; the second-order (2°) and third-order (3°) branches are indicated by *green* and *yellow arrows*, respectively. The *dotted black line* roughly demarcates the inguinal ligament. **B,** Representative multiphoton microscopy (MPM) micrograph of the profunda femoris vein, provided for comparison. **C,** Representative maximum intensity projections (*MIPs*) of second-order intramuscular arteriole (MscA) imaged intact showing the IEL (*Below*) and wall cross-section (*Above*) of each vessel. All cross sections, except for the last, were obtained by reslice of the associated MPM stack. **D,** Representative MIPs of third-order (3°) MscAs imaged intact showing IEL (*Below*) and cross-sectional reslice (*Above*). *Green,* elastic fiber autofluorescence; *red,* collagen second harmonic generation. The images were obtained at 25× magnification. All scale bars = 50 μm. The reslice scale is indicated in both *X* and *Z* directions.

fenestration of gastrocnemius muscle arterioles relative to the popliteal artery upstream and to higher order mesenteric arteries, which might confer improved endothelial communication with the medial VSMCs in some vessels.

We found that as arteries branch with greater degrees of separation from the main elastic conduit vessel and penetrate the skeletal muscle, the IEL thins and has a web-like configuration observed in the arterioles. The arteriolar elastic structure is fundamentally distinct from that of the larger arteries, such that the IEL is no longer a fenestrated sheet but, instead, resembles a wireframe. At the second-order arteriole level, the IEL becomes closer in appearance to that of veins than to that of the aorta. This difference might be of importance. Because new elastic fibers are not created in the mature vertebrate, any arterial wall remodeling would rely on adjusting the preexisting, finite number of elastic fibers present.[5] In the case of large artery occlusion, arterioles that could act as bridges between arterial territories

would remodel into collateral arteries but would simultaneously be limited to their preexisting elastic fiber content.

Both the PFA and the SMA showed, in different forms, greater total fenestration of the IEL than did the other major vessels. IEL fenestrations allow for contact and communication between vascular endothelial cells and VSMCs and passive diffusion of small molecules through the highly insoluble elastic tissue of the IEL. In computational studies, the increased fenestration size can increase IEL permeability to adenosine triphosphate.[7] Kirby et al[10] showed that the larger IEL fenestrations of the first-order arterioles coincided with greater staining of transmembrane proteins involved in endothelium-dependent hyperpolarization compared with the popliteal artery, indicating larger microdomains for myoendothelial Ca^{2+} signaling at fenestrae. In addition, the reduction in IEL fenestration as a result of surgically reduced shear stress can increase the accumulation of macromolecules in the tunica media.[28] Thus, the size and distribution of fenestrae appear to be important determinants of cell—cell communication across lamellae. We, therefore, speculate that certain arteries, such as the PFA and SMA, might require more fenestrae because of a greater need for vascular endothelial cell—VSMC communication.

The arterial system has the capacity for adaptive structural remodeling, driven largely by hemodynamic variables. Chronic hypertension leads to excess matrix deposition, cellular hypertrophy, and contraction of IEL fenestrations, with an end result of increased arterial wall thickening and inward luminal remodeling.[29-31] IEL fenestrations are also the sites of luminal expansion with postnatal arterial growth and outward remodeling in response to increased fluid shear stress.[27,32,33] The common arterial pathologies primarily affect the elastic fibers and collagens, such as aneurysmal disease, arteriosclerosis, and calcinosis. Atherosclerosis is potentiated by signaling of elastin degradation products.[34] Additionally, site specificity of the disease could have a complex relationship with the IEL structure.[35] Greater IEL fenestration could also relate to an increased capacity for remodeling or to a prior outward diameter expansion. The ECM remodeling of muscular arteries and arterioles is a feature of many pathologic conditions, including hypertension.[29] It is possible that the differences in fenestrated elastic lamellar architecture of small arteries contributes to their structural plasticity.

Among all the arteries examined, except for the MscAs, adventitial collagen was similarly relaxed and wavy and maintained a similar organization. The UI correlates with the arterial flow pressure and, thus, the tension on the collagen fibers, with a larger proportion of fibers straightening at higher pressures.[13] Their higher UI showed that MscAs possess adventitial collagen that is generally under greater tension and might take on more of the vessel's wall strain than the larger upstream arteries. This could result from the relative paucity of the elastic fibers present in MscAs compared with the more elastic, axial arteries. Our examination, however, was limited only to visible differences in an excised sample; thus, further examination of the forces experienced by the arterioles and how those forces are distributed among the ECM components is warranted.

Our investigations might have been affected by the necessary manipulation of the tissue. Muscular and elastic arteries were imaged en face from the luminal surface to obtain high resolution scans, given the overall vessel thickness. In contrast, the MscAs were imaged through the intact vessel. Although we were careful to limit the disturbance of the vessel morphology in all situations and to image portions of the artery distant from the edges or flexes in the tissue, the necessary manipulations could have resulted in some distortion. The examinations we have reported represent only a limited subset of locations along the arterial tree and under reduced tension from native conditions. The residual tension from elastic tissues in fixed arterial tissue could have affected the resting morphology and, thus, might explain the increased straightening of adventitial collagen fibers in vessels relatively deficient in elastic tissue, such as the arterioles. Nevertheless, our findings indicate some clear location-specific differences in the arterial ECM architecture.

One limitation of the present study was that we did not have access to normal human arterial samples to compare at similar locations. Numerous studies have documented that the elastic architecture is fairly consistent across mammalian species, with thick fenestrated elastic sheets exemplifying the IEL of larger, elastic arteries.[6,36-38] Another report demonstrated the similarity of small human pericardial vessels to porcine pericardial arteries.[39] In our observation, small nutrient arteries removed from the sciatic artery in the amputation specimens demonstrated an elastic fiber organization that bears resemblance to that of the rat MscAs (Supplementary Fig). The IEL organization appeared similar despite the rat artery being multiple times smaller in size (5-10 times smaller in diameter). A notable difference was the thickness of the IEL elastic fibers, with thicker fibers visible in the human specimens and finer fibers in the rat MscAs. The architecture of the arterial IEL might then be related to the branch point position, rather than to the raw arterial size.

The present study was limited to the analysis of arterial tissues harvested from male rats. It could be of interest for further studies to investigate whether sex-related structural differences exist in baseline arterial tissues. Additionally, it is known that the fenestration size and number can change during development.[27,32] However, the tissue samples collected for the present study were all acquired from rats across the range of ages used;

thus, no systematic variations were present in age or size between the groups.

CONCLUSIONS

Arteries of different sizes and locations along the rat arterial tree displayed significantly different ECM morphology, especially in the elastic lamellae. The baseline morphologies of the ECM might confer susceptibility to the development of pathologies that primarily affect ECM components, such as aneurysmal degeneration or calcification, but also affect adaptive processes, such as outward or inward remodeling. Given elastic fiber vulnerability to calcification, the main line arterial structures with greater elastic tissue content might be more prone to intimal and medial calcification compared with the derivative muscular branches. Also, the more mesh-like or filamentous IEL structure in the muscular branches might result in greater adaptive remodeling capability, such as outward remodeling to form collateral arteries. A clear understanding of the baseline ECM structure might inform our understanding of the pathologic risk associated with different vessels. It is our intent that our findings could offer a baseline to inform further physiologic and pathologic research in the vascular system.

We thank the Center for Biological Imaging at the University of Pittsburgh, and its personnel for the use of their equipment and their expertise. We would especially like to thank Greg Gibson and Dr Simon Watkins for their training and guidance in multiphoton microscopy and image analysis. We also thank Dan Lavage for providing statistical consulting as a part of the Statistical Consulting Center, Department of Statistics, Kenneth P. Dietrich School of Arts and Sciences, University of Pittsburgh.

AUTHOR CONTRIBUTIONS

Conception and design: DM, ET, RM
Analysis and interpretation: DM, NS, EA, RM
Data collection: DM, NS, EA, RM
Writing the article: DM, RM
Critical revision of the article: DM, NS, EA, ET, RM
Final approval of the article: DM, NS, EA, ET, RM
Statistical analysis: DM
Obtained funding: EA, RM
Overall responsibility: RM

REFERENCES

1. Wolinsky H, Glagov S. Structural basis for the static mechanical properties of the aortic media. Circ Res 1964;14:400-13.
2. Harkness ML, Harkness RD, McDonald DA. The collagen and elastin content of the arterial wall in the dog. Proc R Soc Lond B Biol Sci 1957;146:541-51.
3. Roach MR, Burton AC. The reason for the shape of the distensibility curves of arteries. Can J Biochem Physiol 1957;35:681-90.
4. Shapiro SD, Endicott SK, Province MA, Pierce JA, Campbell EJ. Marked longevity of human lung parenchymal elastic fibers deduced from prevalence of D-aspartate and nuclear weapons-related radiocarbon. J Clin Invest 1991;87:1828-34.
5. Wagenseil JE, Mecham RP. New insights into elastic fiber assembly. Birth Defects Res C Embryo Today 2007;81:229-40.
6. Farand P, Garon A, Plante GE. Structure of large arteries: orientation of elastin in rabbit aortic internal elastic lamina and in the elastic lamellae of aortic media. Microvasc Res 2007;73:95-9.
7. Tada S, Tarbell JM. Internal elastic lamina affects the distribution of macromolecules in the arterial wall: a computational study. Am J Physiol Heart Circ Physiol 2004;287:H905-13.
8. Sandow SL, Gzik DJ, Lee RM. Arterial internal elastic lamina holes: relationship to function? J Anat 2009;214:258-66.
9. Ledoux J, Taylor MS, Bonev AD, Hannah RM, Solodushko V, Shui B, et al. Functional architecture of inositol 1,4,5-trisphosphate signaling in restricted spaces of myoendothelial projections. Proc Natl Acad Sci U S A 2008;105:9627-32.
10. Kirby BS, Bruhl A, Sullivan MN, Francis M, Dinenno FA, Earley S. Robust internal elastic lamina fenestration in skeletal muscle arteries. PLoS One 2013;8:e54849.
11. Nissen R, Cardinale GJ, Udenfriend S. Increased turnover of arterial collagen in hypertensive rats. Proc Natl Acad Sci U S A 1978;75:451-3.
12. Rezakhaniha R, Agianniotis A, Schrauwen JT, Griffa A, Sage D, Bouten CV, et al. Experimental investigation of collagen waviness and orientation in the arterial adventitia using confocal laser scanning microscopy. Biomech Model Mechanobiol 2012;11:461-73.
13. Schrauwen JT, Vilanova A, Rezakhaniha R, Stergiopulos N, van de Vosse FN, Bovendeerd PH. A method for the quantification of the pressure dependent 3D collagen configuration in the arterial adventitia. J Struct Biol 2012;180:335-42.
14. Boulesteix T, Pena AM, Pages N, Godeau G, Sauviat MP, Beaurepaire E, et al. Micrometer scale ex vivo multiphoton imaging of unstained arterial wall structure. Cytometry A 2006;69:20-6.
15. Chow MJ, Turcotte R, Lin CP, Zhang Y. Arterial extracellular matrix: a mechanobiological study of the contributions and interactions of elastin and collagen. Biophys J 2014;106:2684-92.
16. Zeinali-Davarani S, Wang Y, Chow MJ, Turcotte R, Zhang Y. Contribution of collagen fiber undulation to regional biomechanical properties along porcine thoracic aorta. J Biomech Eng 2015;137:051001.
17. Sugita S, Matsumoto T. Multiphoton microscopy observations of 3D elastin and collagen fiber microstructure changes during pressurization in aortic media. Biomech Model Mechanobiol 2017;16:763-73.
18. Zoumi A, Yeh A, Tromberg BJ. Imaging cells and extracellular matrix in vivo by using second-harmonic generation and two-photon excited fluorescence. Proc Natl Acad Sci U S A 2002;99:11014-9.
19. Muskopf S. Rat - Circulatory System. Available at: https://www.biologycorner.com/worksheets/rat_circulatory.html. Accessed February 12, 2019.
20. van Baardwijk C, Roach MR. Medial elastin in the thoracic and abdominal aorta of sheep and lambs. Can J Physiol Pharmacol 1983;61:115-9.
21. van Baardwijk C, Barwick SE, Roach MR. Organization of medial elastin at aortic junctions in sheep and lambs. Can J Physiol Pharmacol 1985;63:855-62.
22. Berry CL, Greenwald SE, Rivett JF. Static mechanical properties of the developing and mature rat aorta. Cardiovasc Res 1975;9:669-78.
23. Karrer HE. An electron microscope study of the aorta in young and in aging mice. J Ultrastruct Res 1961;5:1-27.
24. Cleary EG, Cliff WJ. The substructure of elastin. Exp Mol Pathol 1978;28:227-46.
25. Haust MD. Fine fibrils of extracellular space (microfibrils): their structure and role in connective tissue organization. Am J Pathol 1965;47:1113-37.
26. Robertson AM, Duan X, Aziz KM, Hill MR, Watkins SC, Cebral JR. Diversity in the strength and structure of unruptured cerebral aneurysms. Ann Biomed Eng 2015;43:1502-15.
27. Wong LC, Langille BL. Developmental remodeling of the internal elastic lamina of rabbit arteries: effect of blood flow. Circ Res 1996;78:799-805.
28. Guo ZY, Yan ZQ, Bai L, Zhang ML, Jiang ZL. Flow shear stress affects macromolecular accumulation through modulation of internal elastic lamina fenestrae. Clin Biomech (Bristol, Avon) 2008;23(Suppl 1):S104-11.
29. Mulvany MJ. Small artery remodeling in hypertension. Curr Hypertens Rep 2002;4:49-55.

30. Arribas SM, Briones AM, Bellingham C, Gonzalez MC, Salaices M, Liu K, et al. Heightened aberrant deposition of hard-wearing elastin in conduit arteries of prehypertensive SHR is associated with increased stiffness and inward remodeling. Am J Physiol Heart Circ Physiol 2008;295:H2299-307.
31. Briones AM, Gonzalez JM, Somoza B, Giraldo J, Daly CJ, Vila E, et al. Role of elastin in spontaneously hypertensive rat small mesenteric artery remodelling. J Physiol 2003;552(Pt 1):185-95.
32. Roach MR. The pattern of elastin in the aorta and large arteries of mammals. Ciba Found Symp 1983;100:37-55.
33. Masuda H, Zhuang YJ, Singh TM, Kawamura K, Murakami M, Zarins CK, et al. Adaptive remodeling of internal elastic lamina and endothelial lining during flow-induced arterial enlargement. Arterioscler Thromb Vasc Biol 1999;19:2298-307.
34. Gayral S, Garnotel R, Castaing-Berthou A, Blaise S, Fougerat A, Berge E, et al. Elastin-derived peptides potentiate atherosclerosis through the immune Neu1-PI3Kgamma pathway. Cardiovasc Res 2014;102:118-27.
35. VanderLaan PA, Reardon CA, Getz GS. Site specificity of atherosclerosis: site-selective responses to atherosclerotic modulators. Arterioscler Thromb Vasc Biol 2004;24:12-22.
36. Crissman RS. SEM observations of the elastic networks in canine femoral artery. Am J Anat 1986;175:481-92.
37. Lopez-Guimet J, Andilla J, Loza-Alvarez P, Egea G. High-resolution morphological approach to analyse elastic laminae injuries of the ascending aorta in a murine model of Marfan syndrome. Sci Rep 2017;7:1505.
38. Campbell GJ, Roach MR. Fenestrations in the internal elastic lamina at bifurcations of human cerebral arteries. Stroke 1981;12:489-96.
39. Bloksgaard M, Leurgans TM, Nissen I, Jensen PS, Hansen ML, Brewer JR, et al. Elastin organization in pig and cardiovascular disease patients' pericardial resistance arteries. J Vasc Res 2015;52:1-11.

Submitted May 24, 2021; accepted Aug 17, 2021.

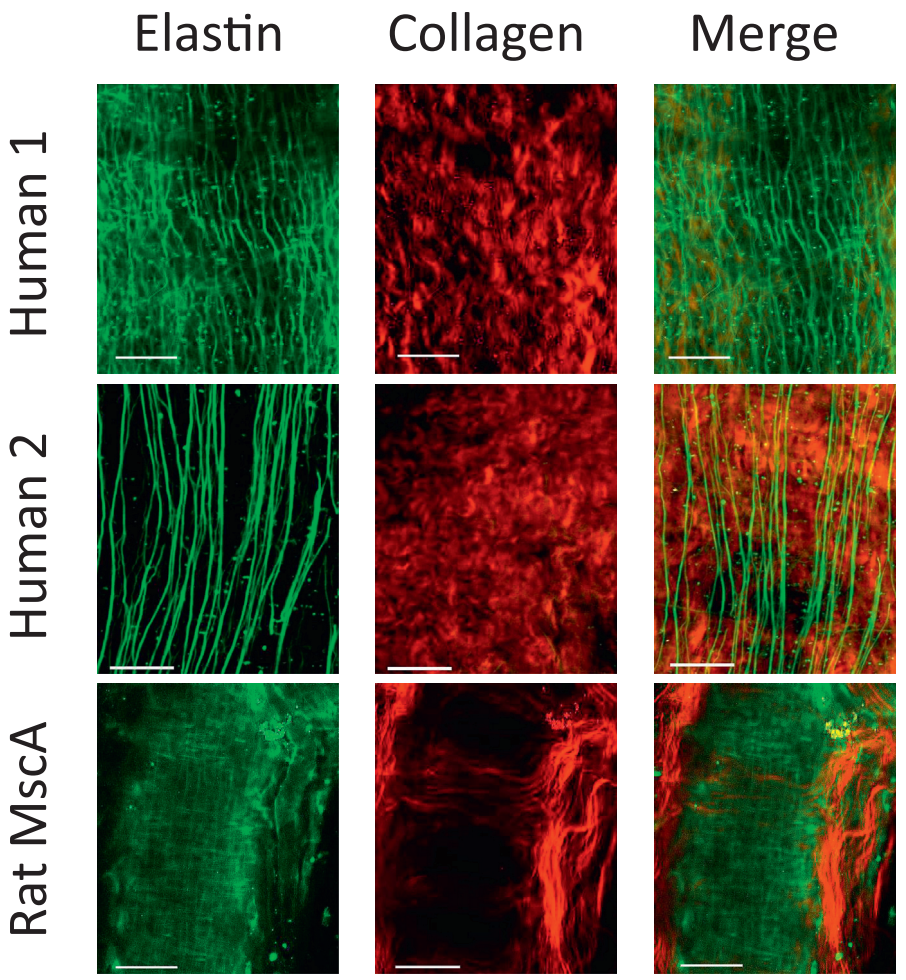

Supplementary Fig. Human small nutrient artery to deep peroneal nerve (*1*) and sciatic nerve (*2*) sampled from lower limb amputation specimens and imaged via multiphoton microscopy (MPM). These vessels have similar structural organizations (filamentous internal elastic lamina [IEL]; wavy collagen morphology) to the small intramuscular arterioles (MscAs) harvested from rats. *Green,* Elastic fiber autofluorescence; *Red,* collagen second harmonic generation. Images were obtained at 25× magnification. Scale bar = 50 μm.